International Journal Of
Industrial Electronics Control and Optimization
Print ISSN: 3517-2645
Online ISSN: 3568-2645
Homepage: https://ieco.usb.ac.ir/

PSO-Based EKF Wheel-Rail Adhesion Estimation

Ramazan Havangi [1]| Maryam Moradi [2]

Faculty of Electrical Engineering and Computer, University of Birjand, Birjand, Iran.[1,2]
Corresponding author's email: Havangi@Birjand.ac.ir

Article Info

Article type:
Research Article

Article history:
Received: 2022-Sep-04
Received in revised form:2023-Jan-09
Accepted: 2023-Feb-02
Published online: 2023-March-15

Keywords:
Adhesion force,
Wheel-rail,
Contact condition estimation,
PSO-based EKF.

ABSTRACT

An ideal traction and braking system not only ensures ride comfort and transportation safety but also attracts significant cost benefits through the reduction of damaging processes in wheel-rail and optimum on-time operation. To overcome the problem of the wheel slip/slide at the wheel-rail contact surface, it is crucial and scientifically challenging to detect adhesion and its changes because adhesion is influenced by different factors. However, critical information this detection provides is applicable not only in the control of trains to avoid undesirable wear of the wheels/track but also in the safety compromise of rail operations. The adhesion level between the wheel and rail cannot be measured directly, but the friction on the rail surface can be measured using measurement techniques. The braking and traction control system can be characterized by estimating wheel-rail adhesion conditions during railway operations. This paper presents the Particle Swarm Optimization (PSO)-based Extended Kalman Filter (EKF) to estimate adhesion force. The main limitation in applying EKF to estimate states and parameters is that its optimality is critically dependent on the proper choice of the state and measurement noise covariance matrices. To tackle this difficulty, a new approach based on the use of the tuned EKF is proposed to estimate induction motor (as a main part of the train moving system) parameters. This approach consists of two steps. In the first step, the covariance matrices are optimized by PSO and then, their values are introduced into the estimation loop. Finally, the superiority of the PSO-based EKF algorithm is verified by making simulations in Matlab and comparing the estimation performances of this technique and EKF. The results prove an acceptable performance in load torque and speed estimation after tuning the covariance matrices and confirm the high accuracy and efficiency of the proposed method.

NOMENCLATURE

a and b: semi-axis length of the contact patch
B and D: reduction factors
C_{11}: Kalker coefficient
C_v: viscous friction
F_a: adhesion force
F_N: normal force between the wheel and rail
G: shear module
$I_{s\alpha}$ and $I_{s\beta}$: $\alpha-\beta$ axis stator currents
c_1 and c_2:self-recognition and social component coefficients
J_{eqv}, J_x: equivalent and wheelset axle moment of inertia
J_g: gearbox moment of inertia
$\psi_{r\alpha}$ and $\psi_{r\beta}$: $\alpha-\beta$ axis rotor flux
J_{wR} and J_{wL}: right and left wheel moment of inertia
k_A and k_S: reduction factors in the adhesion and slip area
L_m: mutual inductance
L_r and L_s: rotor and stator self-inductance
n_i: gear reduction ratio
n_p : number of the pole pairs
N: number of unknown variables or number of samples
P_i: previous best position of each particle
Q and R: process and measurement noise covariance matrixes
r: wheel radius
R_r and R_s: rotor and stator resistance
μ_f: traction coefficient
T_m: motor torque
T_L: load torque
V: longitudinal velocity
$v(t)$ and $w(t)$: measurement and process noise
V_i, X_i: velocity and position of ith particle
w: inertia weight factor
ϵ: gradient of tangential stress
ξ: creepage between the wheel and rail
$\omega_{m,}\omega_w$: motor and angular velocity

I. Introduction

Locomotive design, which was introduced more than 200 years ago, is still developing and in progress. Based on the type of energy usage, railway vehicles are divided into three classes: steam, diesel-fueled, and electric. In steam locomotives, steam energy is provided by the combustion of fuels. Since steam locomotives cannot be loaded with over a certain amount of fuel, they cannot operate at long distances. So, the application of the steam system in this vehicle has been completely obsolete. The source of energy in diesel-fueled locomotives is diesel motors. According to the fuel tank, a diesel train that pulls ten wagons can take approximately 600-700 km distance. Unlike these two types, electric locomotives have no refueling problems, so they are suitable for traveling long distances. Another advantage of these locomotives is that they are the most economical locomotives because of their tractive effort.

Progress in science and technology, especially in the field of computer modeling, has allowed the adoption of new and advanced forms of traction systems for railway vehicles. However, the performance of the locomotive traction system is limited by the adhesion condition between the wheel and the rail. Adhesion is the key element for determining optimal traction performance. Moreover, adhesion affects the passengers' comfort, the safety of transportation equipment, and railway vehicles' energy management. Wheel shape and size and rail contact area directly influence the motion of railway vehicles. The Hertzian theory is one of the methods widely used to find the contact patch shape and size. This theory includes some assumptions such as non-conformal elliptical contact (valid if dimensions of the contact area are smaller than the curvatures of surfaces), frictionless surfaces, and elastic half-spaces. It is worth noting that the dynamics of railway wheelsets are influenced by different factors. This impactability and uncertain variations in the contact condition complicate the mechanical system of railway wheelsets significantly.

The interaction of the vehicle and track is affected by four main factors: suspension characteristics, metallurgy, contact mechanics, and friction. The wheel-rail interaction is the most important issue in the dynamics of railway vehicles. Any changes in the contact condition can trigger subsequent changes in the braking and traction responses of the rail vehicle [1], especially when the rail and/or wheel contact surfaces are subject to environmental factors such as dirt [2], water, deliberately applied friction modifiers [3], weather conditions [4], or contact surface temperatures [5-7], leading to the well-known problem of low adhesion. Slip/slide, which can potentially cause severe wear of wheel and rail surfaces and increase mechanical stress in the system, is caused by low adhesion. Wheels slip in traction or slide in braking if they deliver a higher force to the rail than they can transmit. Meanwhile, instability and inconsistent traction performance, which cause problems in train schedules, are negative effects of low adhesion. If creepage at the wheel-rail interface increases, the temperature will increase in the contact areas and it will decrease the coefficient of friction, resulting in the creation of flatness, shelling, and skid marks on the wheels and rails, which also suffer from wheel burns and deterioration caused by damaged wheels. As a result, the rails need regrinding, and the wheelsets need reprofiling or replacing, which imposes additional costs on the rail industry. Adhesion estimation in wheel-rail contact area during train operation, which is an important task for railway industries, is a multifaceted process as it depends on several operational factors that influence nonlinear processes at the wheel-rail contact interface. To characterize the braking and traction, which are key elements of performance and safety issues, accurate information about the adhesion is necessary [8].

There are many approaches proposed by researchers to studying adhesion. Investigating the lateral dynamics, specific types of friction conditions (dry or wet), or single wheelsets are methods mentioned in [9-11] for surveying the wheel-rail interface. To control the wheel rotational acceleration below a pre-defined threshold, controlling the measured slip ratio (relative speed between the train and wheel) is noted in commonly used wheel slip protection schemes [12-14]. The operational rail self-cleaning mechanism [15], axle load distributions, vehicle speed, and track irregularities are other train operational factors that researchers consider in adhesion estimation. Additionally, rail vehicle design has a significant effect on adhesion [16]. In [17], a single wheelset velocity was used as Kalman filter input to detect adhesion force for slip control purposes. This model has, also, been applied to detect wheel slip/slide and re-adhesion control of AC traction motors in railway applications [18]. To suppress the slide and slip and adjust the torque command, a multiple-induction motor single inverter has been investigated to estimate the adhesion force [19,20]. Extended Kalman filter (EKF)-based estimation of creepage, creep force, and friction coefficient between the wheel and rail surfaces by utilizing the stator voltage, current, and speed of the traction AC motor was proposed in [21]. Another method to detect slip velocity is multi-rate EKF state identification. In this method, traction motor load torque is identified by combining the multi-rate method and the EKF method. Faster detection of slip and reliability and traction performance improvement are benefits of this approach [22].

Estimation of the rotor fluxes, currents, and motor speed for direct vector control of induction motors in the implementation of the EKF algorithm was proposed in [23]. For the system to operate at the optimal state, proper selection of measurement noises and covariance matrices is an important problem associated with the use of EKF. It is worth noting that both matrices are not known, especially

since it is very difficult to define the system noise. Therefore, these matrices are often used as parameters for tuning. The adjustment can be made by using evolutionary algorithms or a trial-and-error approach [24]. Adhesion can be estimated by focusing on longitudinal dynamics and associated adhesion effects. In this method, an observer is designed, and nonlinear wheel-rail contact is considered. To cover this nonlinearity, EKF was combined with a parameter estimator [25]. It should be noted that EKF estimation is directly related to the correct selection of system and measurement noise covariance matrices. Due to the unknown stochastic properties of the corresponding noises in EKF, it is not possible to obtain the mathematical relationship between the EKF performance and the noise covariance matrices. Therefore, researchers have proposed different methods to determine these matrices in the literature. These methods have classified the matrices into constant and dynamic. In the first classification, matrices are determined by the trial-and-error method [26-29]. This approach is not only time-consuming but also does not yield optimum results for the whole speed range. In [30], an unscented Kalman filter (UKF) was employed for IM state estimation and the results were compared with EKF, which showed that at the beginning of the simulation, UKF outperformed EKF but when the input torque was changed, EKF started to outperform UKF. The next group of studies has performed off-line optimization of these matrices by focusing on heuristic algorithms such as differential evolution [31-32] and genetic algorithms [33].

Unlike conventional optimization algorithms such as Newton-Rapson and Levenberg-Marquardt, which require mathematical expressions and their derivatives, heuristic algorithms provide derivative-free global optimization using only fitness functions and fitness values [33]. Because of the offline optimization process, the optimization method is time-consuming like the trial-and-error method. Meanwhile, the operating conditions of the induction motor affect these matrices, so they must be updated depending on the working conditions. Therefore, the second group of studies [34-37] has proposed the capability of online updating of these matrices. Some of these studies [35,37] have used the fuzzy logic approach to update these matrices. Knowledge and experience of an expert are two key factors to achieve high performance estimations with this method, so its design process is quite complicated.

Model-based adhesion estimation (which is based on the contact forces and moments analysis) is another method used in the literature. Due to the dependence of creep forces and moments on the level of track irregularities, it is difficult to illustrate adhesion conditions without prior knowledge of the track irregularities. To solve such a problem, the estimation of adhesion conditions based on the eigenvalue analysis without prior knowledge of the track irregularity level was proposed [38]. The non-model-based estimation scheme compares the dynamic responses of leading and trailing wheelsets using the yaw positions of the leading and trailing bogies [39]. In general, simulation methodology used for rail vehicles' traction system can be divided into the following simulation stages: simulation of the mechanical system [40-42], simulation of the longitudinal dynamics of the train [40-41], simulation and modeling of the electrical and traction control systems [43-44], creep force modeling at the wheel-rail interface [45-50], simulation of the full mechatronic system of a locomotive [41,51-52], and validation and verification of the results [40,53-54].

PSO is an evolutionary computation method that is used to optimize nonlinear systems [55]. This approach was first introduced in [56], and since then, it has been considered one of the most popular optimization methods in the literature. In [57], the PSO algorithm is used to optimize the objective function to reach the best parameters and variables of controllers. In [58], the use of the PSO algorithm in railway studies is reviewed, but the use of PSO for adhesion and creep force modeling is not mentioned. PSO is preferred due to its simplicity and the high nonlinearity in adhesion and creep force models. To demonstrate the level of agreement between adhesion and creep force models and measurements, PSO-based parameterization of adhesion and creep force models is proposed in [59]. Swarm intelligence-based adhesion estimation algorithm allows determining the adhesion optimum between wheel and rail. Therefore, the reference slip value for the controller can be determined according to the adhesion conditions, which leads to an effective wheel slip control performance [60].

Among the state observer mentioned above, EKF is an accurate estimator. The disadvantage of EKF is that its effectiveness heavily depends on the covariance matrices of the measurement and system noises, which are critical parameters for torque and speed estimation of induction motors and usually could not be acquired accurately. Thus, several intelligent optimization algorithms have been proposed to enhance the EKF performance. In this paper, the PSO algorithm is employed to optimize EKF for torque (which has a linear relation with adhesion force) and estimate the speed of the induction motor. The main contributions of this paper are (1) the formulation of a mathematical model for the torque estimation of an induction motor for wheel-rail adhesion estimation, (2) the successful employment of the PSO algorithm to optimize EKF covariance matrices, and (3) the construction and implementation of a simulation model in Matlab to evaluate the performance of PSO-EKF. The effectiveness of the proposed approach for adhesion estimation is verified through simulation experiments, and its superiority in the estimation of variables compared to conventional EKF is proved.

The rest of this paper is organized into five sections. Section II introduces the principle concepts of PSO. Section

III gives the details of the traction system and the sixth-order mathematical model of the induction motor. The PSO-based EKF framework is presented in Section IV. Section V provides the details of the experimental results in the implementation of EKF. Finally, Section VI presents the conclusion.

II. Particle Swarm Optimization Concepts

PSO is a metaheuristic algorithm that optimizes a problem by iteratively trying to improve a candidate solution with regard to a given measure of quality. PSO is motivated by the intelligent collective behavior of some animals, such as bird flocking and fish schooling. This optimization algorithm exploits the concepts of social sharing of information in which the population is called a swarm, and each individual in the swarm is called a particle. In PSO, to improve the results for a defined objective function, an iterative procedure is followed and the particles move in the search space based on the reasoning as follows.

First, they evaluate their fitness continuously and in each iteration, memorize the best position that they have ever had in their movement history. Second, knowing the position of the best particle in the swarm, particles move in the n-dimensional space, foraging the solution.

Particles in the swarm are in communication with each other and update the mentioned parameters in each iteration. While moving toward the best position, they change their position and velocity based on the local and global best information. Local best refers to the best position of each particle in its movement history, and the best position of the whole group is called global best which is updated in each iteration. Therefore, the whole group would have sufficient knowledge about the position of the new global best, if the best position is changed. All the particles in the swarm search areas near the global best and try to move toward them. This phenomenon is called convergence.

Small values of the inertia weight allow all particles to reduce their speed so that when they reach the area of the global best, their speed converges to zero. When unpleasant convergence occurs, we can give the particles a new set of initial values to get rid of this unpleasant situation. PSO has two advantages over the GA algorithm. First, in PSO, particles decide about the next movement in the space by using their history and the best of the group history but in GA, transferring the knowledge of the current group to the next is completely hereditary. It is obvious that random procedures of cross-over and mutation affect this inheritance, and pure knowledge is not transferred from one generation to the next; hence, PSO is more reliable and faster than GA. Second, death and reborn of the particles in GA, in each iteration, cause computational burden on the system to arise whereas in PSO, the population of the particles is constant and particles only update their position and velocity, so there is no computational burden problem.

III. Traction System and Discrete-Time Mathematical Model

In the simulated system used in this research, a wheelset with two wheels is driven by an AC induction motor through a gear set. The details of the traction system are presented in Fig.1.

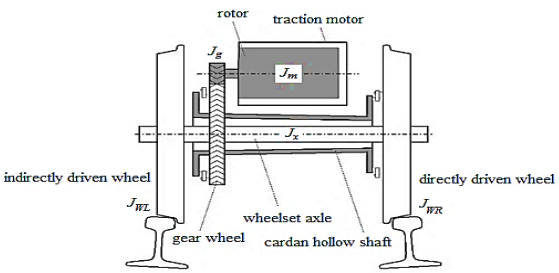

Fig. 1. The schematic of the traction system.

The wheels are driven by the creep forces generated at the contact patch between the wheels and the rail. Hence, the dynamic equations are given as:

$$\omega_w = \frac{\omega_m}{n_i} \quad (1)$$

$$\frac{d\omega_m}{dt} = \frac{T_m - T_L}{J_{eqv}} \quad (2)$$

where ω_w is the wheel's angular velocity, ω_m is the motor's angular velocity, n_i is the gear reduction ratio, T_m is the motor torque, and T_L and J_{eqv} are the load torque and the equivalent moment of inertia, respectively represented as:

$$T_m = \frac{n_p L_m}{L_r}(I_{s\beta}\psi_{r\alpha} - I_{s\alpha}\psi_{r\beta}) \quad (3)$$

$$T_L = \frac{2rF_a}{n_i} \quad (4)$$

$$J_{eqv} = J_m + \frac{J_g + J_x + J_{wR} + J_{wL}}{n_i^2} \quad (5)$$

where Fa is the longitudinal creep force or adhesion force of a single wheel and J_g, J_x, J_{wR}, J_{wL} are the moment of inertia of the gearbox, wheelset axle, right wheel, and left wheel, respectively.

In this paper, the sixth-order rotor flux-based induction motor model is used in the EKF algorithm to estimate $I_{s\alpha}$, $I_{s\beta}$, $\psi_{r\alpha}$, $\psi_{r\beta}$, ω_m, and T_L. In this modeling, the state variables are stator current, rotor flux, angular velocity of the motor, and load torque. The state space representation of such a model can be written as follows [61]:

$$\frac{dx(t)}{dt} = AX(t) + Bu(t) + \mathrm{w(t)} \quad (6)$$

$$y(t) = CX(t) + v(t) \quad (7)$$

$$X = [I_{s\alpha} \quad I_{s\beta} \quad \psi_{r\alpha} \quad \psi_{r\beta} \quad \omega_m \quad T_L]^T \quad (8)$$

$$y = [I_{s\alpha} \quad I_{s\beta}]^T \quad (9)$$

$$u = [u_{s\alpha} \quad u_{s\beta}]^T \quad (10)$$

$$A=\begin{bmatrix} -\left(\frac{R_s}{\sigma L_s}+\frac{L_m^2 R_r}{\sigma L_s L_r^2}\right) & 0 & \frac{L_m R_r}{\sigma L_s L_r^2} & \frac{L_m}{\sigma L_s L_r} n_p \omega_m & 0 & 0 \\ 0 & -\left(\frac{R_s}{\sigma L_s}+\frac{L_m^2 R_r}{\sigma L_s L_r^2}\right) & -\frac{L_m}{\sigma L_s L_r} n_p \omega_m & \frac{L_m R_r}{\sigma L_s L_r^2} & 0 & 0 \\ \frac{R_r L_m}{L_r} & 0 & -\frac{R_r}{L_r} & -n_p \omega_m & 0 & 0 \\ 0 & \frac{R_r L_m}{L_r} & n_p \omega_m & -\frac{R_r}{L_r} & 0 & 0 \\ \frac{-3 n_p L_m}{2 J_{eqv} L_r} \psi_{r\beta} & \frac{3 n_p L_m}{2 J_{eqv} L_r} \psi_{r\alpha} & 0 & 0 & -\frac{C_v}{J_{eqv}} & -\frac{1}{J_{eqv}} \\ 0 & 0 & 0 & 0 & 0 & 0 \end{bmatrix} \quad (11)$$

$$B=\begin{bmatrix} \frac{1}{\sigma L_s} & 0 \\ 0 & \frac{1}{\sigma L_s} \\ 0 & 0 \\ 0 & 0 \\ 0 & 0 \\ 0 & 0 \end{bmatrix} \quad (12)$$

$$C=\begin{bmatrix} 1 & 0 & 0 & 0 & 0 & 0 \\ 0 & 1 & 0 & 0 & 0 & 0 \end{bmatrix} \quad (13)$$

$$\sigma = 1 - \frac{L_m^2}{L_s L_r} \quad (14)$$

where R_s is the stator resistance, R_r is the rotor resistance, L_s is the stator self-inductance, L_r is the rotor self-inductance, L_m is the mutual inductance, n_p is the number of the pole pairs, σ is the leakage coefficient, and C_v is the viscous friction. The extended model of IM can be represented by (15) and (16).

$$\begin{bmatrix} \dot{I}_{s\alpha} \\ \dot{I}_{s\beta} \\ \dot{\psi}_{r\alpha} \\ \dot{\psi}_{r\beta} \\ \dot{\omega}_m \\ \dot{T}_L \end{bmatrix} = A \begin{bmatrix} I_{s\alpha} \\ I_{s\beta} \\ \psi_{r\alpha} \\ \psi_{r\beta} \\ \omega_m \\ T_L \end{bmatrix} + \begin{bmatrix} \frac{1}{\sigma L_s} & 0 \\ 0 & \frac{1}{\sigma L_s} \\ 0 & 0 \\ 0 & 0 \\ 0 & 0 \\ 0 & 0 \end{bmatrix} \begin{bmatrix} U_{s\alpha} \\ U_{s\beta} \end{bmatrix} + w(t) \quad (15)$$

$$\begin{bmatrix} I_{s\alpha} \\ I_{s\beta} \end{bmatrix} = \begin{bmatrix} 1 & 0 & 0 & 0 & 0 & 0 \\ 0 & 1 & 0 & 0 & 0 & 0 \end{bmatrix} \begin{bmatrix} I_{s\alpha} \\ I_{s\beta} \\ \psi_{r\alpha} \\ \psi_{r\beta} \\ \omega_m \\ T_L \end{bmatrix} + v(t) \quad (16)$$

where $w(t)$ and $v(t)$ are the process and measurement noise, respectively.

$$F_a = \frac{2 F_N \mu_f}{\pi} \left(\frac{k_A \epsilon}{1+(k_A \epsilon)^2} + \arctan(k_S \epsilon)\right),\ k_S \le k_A \le 1 \quad (17)$$

F_a at the wheel-rail contact is modeled by Polach's method [62], which has been widely used in commercial codes owing to its short computational time and satisfactory accuracy compared with other methods.

$$\epsilon = \frac{G \pi a b C_{11}}{4 F_N \mu_f} \quad (18)$$

$$\xi = \sqrt{\xi_x^2 + \xi_y^2} \qquad \xi \approx \xi_x,\ \xi_y \approx \quad (19)$$

where F_N is the normal force between the wheel and rail, μ_f is the traction coefficient, k_A and k_S are different reduction factors in the areas of adhesion and slip, respectively, G is the shear module, a and b are the semi-axis lengths of the contact patch, C11 is the Kalker coefficient, and ξ is the creepage between the wheel and rail. In this paper, the creepage terms contain only the longitudinal component, and the lateral dynamics of the system are neglected. This creepage was calculated by the following equation [63]:

$$\xi = \frac{\omega_w r - V}{V} \quad (20)$$

where V is the longitudinal velocity of the train. The traction coefficient in (17) depends on the slip velocity (ξV) and friction coefficient, which is expressed by the following equation:

$$\mu_f = \mu_0((1-D)e^{-B\xi V} + +D \quad (21)$$

where D and B are reduction factors under different friction coefficients.

IV. Wheel-rail Adhesion Estimation using PSO- EKF

In this paper, we attempt to find the best linear estimation of the state vector of the induction motor to estimate the adhesion force between the wheel and rail surfaces. The state and measurement equations are given as follows:

$$F_e(k) = \frac{\partial f_e(x_e(k).u_e(k))}{\partial x_e(k)}\Big| \hat{x}_e(k).\hat{u}_e(k) \quad (22)$$

$$F_u(k) = \frac{\partial f_e(x_e(k).u_e(k))}{\partial u_e(k)}\Big| \hat{x}_e(k).\hat{u}_e(k) \quad (23)$$

$$P^-(k+1) = F_e(k) P_k(k) (F_e(k))^T + F_u(k) D_u(k) (F_u(k))^T + Q(k) \quad (24)$$

$$K(k) = P^-(k+1) H^T (H P^-(k+1) H^T + R(k))^{-1} \quad (25)$$

$$\hat{x}_e(k+1) = \hat{f}_e\left(x_e(k).\hat{u}_e(k)\right) + K(k)(z(k) - H\hat{x}_e(k)) \quad (26)$$

$$P(k+1) = (I - K(k)H) P^-(k+1) \quad (27)$$

where Q and R are the covariance matrixes of process and measurement noise and I is the unit matrix symbol. Due to the uncertainty of Q and R, their values are obtained by trial-and-error methods which are very tedious procedures. The values of these matrixes have a significant effect on the EKF output. This is considered a defect for this type of estimator. To overcome this problem and to avoid the

computational complexity of the trial-and-error method, we use both EKF and PSO techniques and try to tune Q and R. In the literature, the trial-and-error method is used to tune the covariance matrices of EKF, which is a very laborious task. To surmount this problem, genetic algorithms have been used to optimize and tune the two matrices automatically [64]. In this work, EKF is designed and implemented for the estimation of motor torque with randomly selected values of Q and R. To optimize the EKF-based torque estimation of the induction motor and avoid the difficulty of determining Q and R, an alternative method is used in which the two matrices are tuned and optimized based on PSO. This approach consists of two steps. It first allows finding the optimal values of Q and R, and then these values are injected into the EKF estimator to estimate motor parameters.

In PSO, all particles fly all over a multidimensional search space and adjust their position according to their own experience and that of neighbors. The position of the i^{th} particle (X_i), the previous best position of each particle (P_i), and the individual velocity (V_i) that each particle moves in the swarm are defined as follows:

$$X_i = (x_{i1}, x_{i2}, \ldots, x_{iN}) \quad (28)$$

$$P_i = (p_{i1}, p_{i2}, \ldots, p_{iN}) \quad (29)$$

$$V_i = (v_{i1}, v_{i2}, \ldots, v_{iN}) \quad (30)$$

where i and N denote the i^{th} particle and dimension of the problem or the number of unknown variables, respectively. In PSO, initialization is done with a group of random particles and it is tried to find the optimum value by updating generations. Each particle is updated by two best values in every iteration: 1) the best position that each particle achieved so far during the optimization process or pbest and 2) the best position ever achieved by any particle in the population or gbest. After finding the two best values, the position and the velocity of each particle in the k^{th} iteration are updated by the following equations in the inertia weight approach (IWA):

$$v_i(k+1) = \underbrace{w.v_i(k)}_{\text{Current motion}} + \underbrace{c_1.r_1(k).(p_i(k) - x_i(k))}_{\text{Personal influence}} + \underbrace{c_2.r_2(k).(p_g(k) - x_i(k)}_{\text{Social influence}} \quad (31)$$

$$x_i(k+1) = x_i(k) + v_i(k+1) \quad (32)$$

where w is the inertia weight factor that controls the impact of the previous velocity on the new velocity, v_i is the velocity of the i^{th} particle, c_1 and c_2 are the positive constants, called coefficients of the self-recognition and social component and determine which controls the relative impact of the local and the global knowledge on the movement of each particle respectively, r_1 and r_2 are two random numbers used to maintain the diversity of the population and uniformly distributed in the interval [0,1], p_i is pbest of the i^{th} particle, x_i is the current position of the i^{th} particle, and p_g is gbest of the swarm.

The velocity is updated by Eq. (31) from the previous velocity to the new one. The new position of each particle is determined by Eq. (32) which is the sum of the previous position and the new velocity. Tuning of Q and R is necessary to achieve the best estimations. Any changes in these two parameters affect both the steady-state and transient duration operation of EKF. If Q increases, large state noises or uncertainties in the machine will be inevitable, which will cause higher Kalman gain, faster EKF transient performance, and more heavily weighted measurements. Strong noise measurements, weighted less noise, decreased Kalman gain, and slower transient performance are the consequences of increased R.

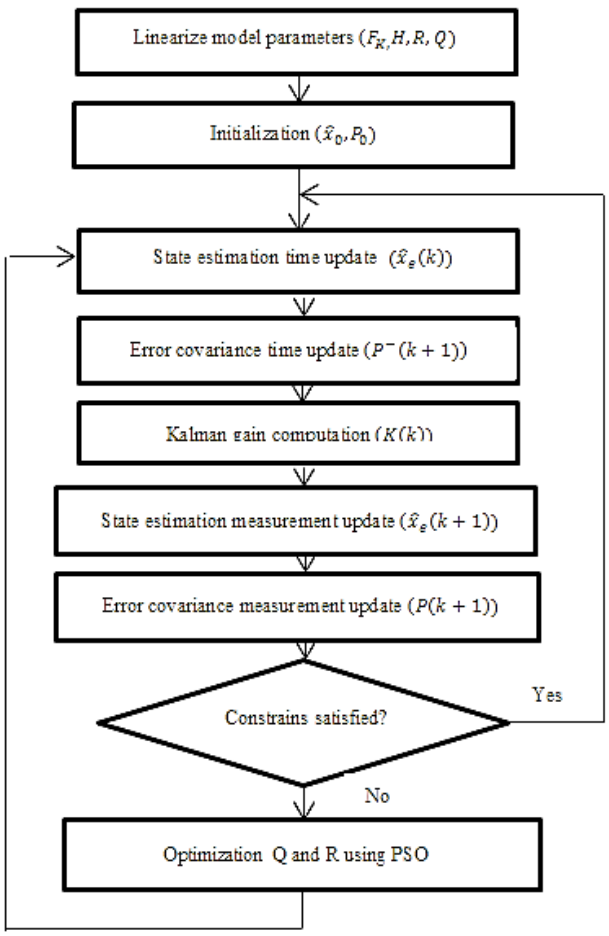

Fig 2. The PSO-EKF algorithm flowchart

Therefore, in the first step, the optimal values of Q and R are found. Then, these values of Q and R are injected into the EKF estimator to estimate the rotor speed and torque of the induction motor. For comparison purposes, the performance of EKF is evaluated by the fitness function between the estimated current and the actual stator current as Eq. (33). The manual adjustment of EKF is simple to implement, but the process is time-consuming. So, to obtain satisfactory

estimation performance, an experienced operator is needed. In this work, PSO- EKF is used to get the optimal covariance matrices. In the optimization of covariance matrices, the elements of system noise and measurement noise covariance matrices are regulated under some performance index, i.e. fitness function. The stator current can be measured by using current sensors. Smaller differences between the measured and the estimated current imply more accurate torque and speed estimation of the induction motor. These difference values of stator current can be adopted as the fitness function,
which must be minimized as below:

$$\min \ J=\frac{1}{N}\sum_{k=0}^{N}\|i_s(k)-\hat{\imath}_s(k)\|_2^2 \qquad (33)$$

where N is the number of samples involved in the optimization, i_s is the actual stator current, $\hat{\imath}_s$ is the estimated stator current, and $\|.\|_2$ is the Euclidean distance.

PSO has six main steps. 1) Each particle in the swarm starts to move with random velocity and position in N dimensions of the problem space. 2) Fitness of each particle is evaluated. 3) Velocity and position of each particle are changed according to Eq. (31) and (32), respectively. 4) The lbest (local best) and gbest will be updated if necessary; the updated position of each particle is evaluated according to its fitness. 5) If the criterion is met, the optimization process ends; otherwise, it goes to step 3 and the steps are repeated. 6) The best global solution results from this optimization process.

In this paper, the PSO-EKF method is utilized to evaluate the accuracy compared with EKF in estimating variables. The method is composed of two steps. At first, a PSO-based EKF structure is presented which allows for finding the optimal values of Q and R. In the second step, these optimal values are injected into the EKF estimator to estimate the torque, which leads to adhesion force estimation. The block diagram of the PSO-EKF parameter estimation system is illustrated in Fig.2. Also, the pseudo-code for PSO-EKF is shown in Appendix A.

V. Results and simulation

This section aims to evaluate the accuracy of EKF in estimating the variables. To demonstrate the performance of the proposed PSO-EKF approach, adhesion force in different wheel-rail contact conditions and induction motors are simulated using Matlab software. Note that the sampling period we used to write our codes in Matlab language is 10^{-3} s.

To simulate dry, wet, low, and very low contact conditions between the wheel and rail, friction coefficients are designed as follows:

$$\mu_0 = \begin{cases} 0.55 & t < 10 \\ 0.3 & 10 \le t < 20 \\ 0.06 & 20 \le t < 30 \\ 0.03 & 30 \le t < 35 \end{cases}$$

Q and R can be given as:
Q = diag ([1e-11 1e-9 1.39e-12 1e-9 1.85e-6 1.42e-6])×0.02
R = diag ([4e-3 4e-3])

The values of k_A, k_S, D, and B under different friction conditions are listed in Table 1.

TABLE 1
POLACH MODEL PARAMETERS UNDER DIFFERENT FRICTION CONDITIONS [18]

Model parameter	Wheel–rail conditions			
	Dry	Wet	Low	Very Low
k_A	1	1	1	1
k_S	0.4	0.4	0.4	0.4
D	0.6	0.2	0.2	0.1
B	0.4	0.4	0.4	0.4

The parameters used in the simulation are listed in Table 2. Fig.3 shows the curves of the adhesion force versus creepage in different wheel-rail contact conditions. As is seen in this figure, the creepage curve has a nonlinear characteristic. The area on the right side of the peak is called the creepage zone and the area on the left side of the peak is the adhesion zone.

TABLE 2
PARAMETERS AND VALUES USED IN THE SIMULATION

f (Hz)	L_S(H)	L_m(H)	L_r(H)	R_r (Ω)	R_S (Ω)
50	0.1004	0.0915	0.0969	1.294	1.54
r (m)	G ($\frac{N}{m^2}$)	C_{11}	F_N (kN)	J_{eqv} (kg.m^2)	C_v ($\frac{N.m}{rad.s}$)
0.34	8.4×10^{10}	4.12	50	0.07	0.015
V($\frac{m}{s}$)	b (m)	n_p	a (m)	n_i	
15	0.0075	3	0.0015	6.92	

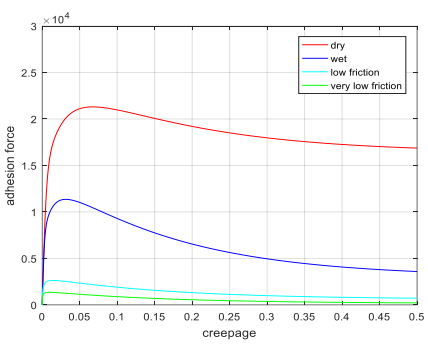

Fig.3. Adhesion force–creepage curves.

The creepage zone is the non-stable part of the curve, and adhesion decreases when the creepage increases. On the other hand, the adhesion zone is the stable part of the curve, in which adhesion increases when the creepage increases. Increasing the creepage, the slip region increases versus the

stick region.

In the next step, induction motor parameters are estimated using EKF, and their actual and estimated trajectories are compared separately to check the degree of estimation accuracy and convergence. Estimated stator currents in $\boldsymbol{\alpha}$ and $\boldsymbol{\beta}$ frames ($\hat{\boldsymbol{I}}_{\boldsymbol{s\alpha}}$, $\hat{\boldsymbol{I}}_{\boldsymbol{s\beta}}$) with their actual trajectory are presented in Figs.4 (a) and (b), respectively. The trajectory of the estimated and actual rotor fluxes in $\boldsymbol{\alpha}$ and $\boldsymbol{\beta}$ frames ($\hat{\boldsymbol{\psi}}_{\boldsymbol{r\alpha}}$,$\hat{\boldsymbol{\psi}}_{\boldsymbol{r\beta}}$)are displayed in Figs.5 (a) and (b), respectively.

It can be seen in Figs.4 and 5 that the presence of an error in the estimated trajectories of the stator current and rotor flux relative to the actual trajectories of these two variables is inevitable.

The estimated and actual motor speeds (ω_m,$\hat{\omega}_m$) are given in Fig.6 according to which the EKF estimator tracks the speed trajectory with a lower bound of error and converges fast. Despite good convergence, according to the simulation observations, any changes in the values of the noise and process covariance matrices will lead to significant changes in the estimated trajectory of motor speed.

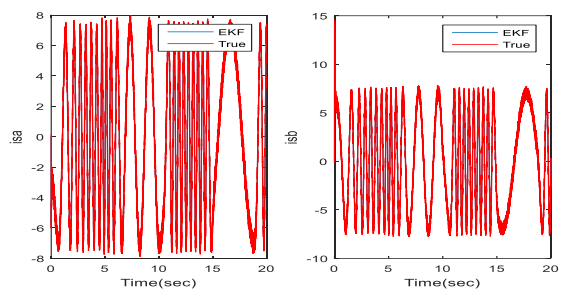

Fig.4.The trajectories of the estimated and actual motor currents (a) in α axis (b) in β axis.

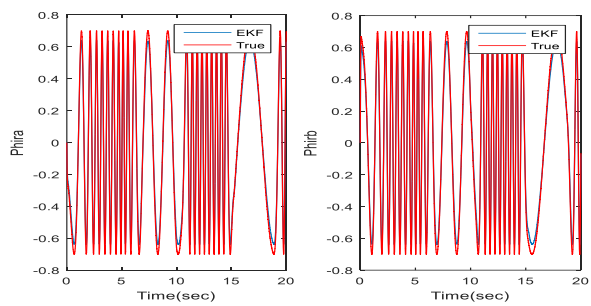

Fig.5. The trajectories of the estimated and actual rotor fluxes (a) in α axis (b) in β axis

The trajectory of the estimated and actual load torque (T_L , $\hat{T}_L$) is presented in Fig.7. According to the linear relationship between the load torque and the adhesion force expressed in Eq. 4, the estimated adhesion force trajectory is obtained as shown in Fig.8. Contrary to the relatively good convergence between the estimated and actual motor speed trajectory, we are faced with a high error band in the estimated and actual load torque trajectory. To overcome this error and achieve the desired trajectory, it is necessary to change the system and process noise covariance matrices' values. Achieving such values will be possible using trial and error, which is a time-consuming approach.

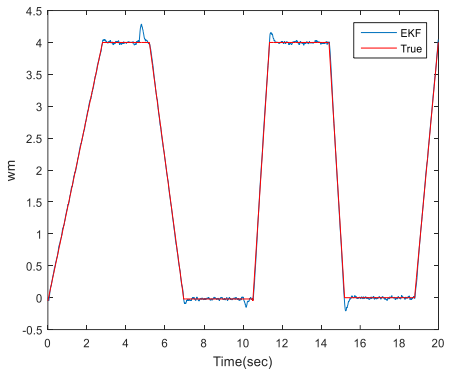

Fig.6. The trajectory of the estimated and actual motor speed.

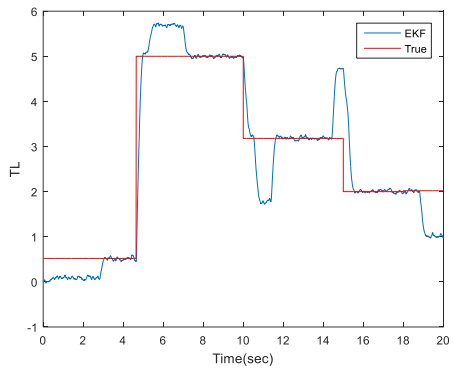

Fig.7. The trajectory of the estimated and actual load torque.

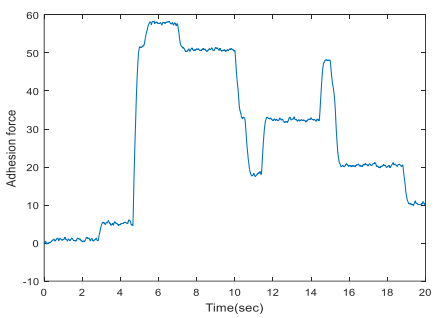

Fig.8. The trajectory of the estimated adhesion force.

It can be seen from the simulation results that estimating the variables using EKF cannot provide the necessary accuracy and convergence in load torque and speed estimation, which are the most important factors in estimating wheel and rail adhesion. As a result, using an integrated method to eliminate these drawbacks can play an essential role in achieving the desired result. As was already mentioned, the key problem of EKF is that the covariance matrices Q and R have a great effect on the estimation results. Bad choices of these two matrices will lead to large estimation errors or the result of estimation divergent. Tuning of Q and R will yield the best estimations.

In this section, we try to tune and optimize Q and R based on the PSO algorithm. It is worth noting that the convergence of the PSO method to the optimal solution depends on the three parameters of c1, c2, and w in Eq. (31). During simulations, c1, c2, and w are set to 2, 2, and 1, respectively and swarm population is set to five particles. In the following, we will show the simulation results obtained by our proposed approach PSO- EKF. The optimized parameters of EKF obtained by our proposed approach are as follows:

QR = [(1e-8)/5 (1e-6)/5 (1.39e-9)/5 (1e-6)/4
(1.85e-3)/4 (1.42e-2)/4 4e-3 4e-3]×3e-6

PSO- EKF stator currents in α and β frames with their actual trajectories are presented in Figs.9 (a) and (b), respectively. The trajectories of PSO- EKF and actual rotor fluxes in α and β frames are displayed in Figs.10 (a) and (b), respectively.

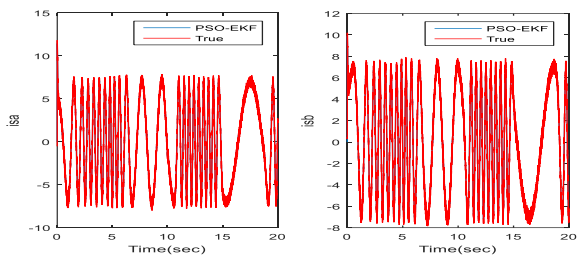

Fig.9. The trajectories of the PSO- EKF and actual motor currents (a) in α axis (b) in β axis.

It can be seen in Figs.9 and 10, the trajectories of the stator current and rotor flux relative to the actual trajectories of these two variables have suitable convergence.

PSO-EKF and actual trajectories of induction motor speed are depicted in Fig.11. The trajectories of - EKF and actual load torque are presented in Fig.12.

Figs.11 and 12 show that the proposed estimator tracks the speed and torque trajectories with a lower bound of error and converges fast. As can be seen, when sudden changes happen in the speed and torque, the error changes in a narrow band interval. Therefore, the tuned estimator tracks the state trajectories with higher precision and converges fast.

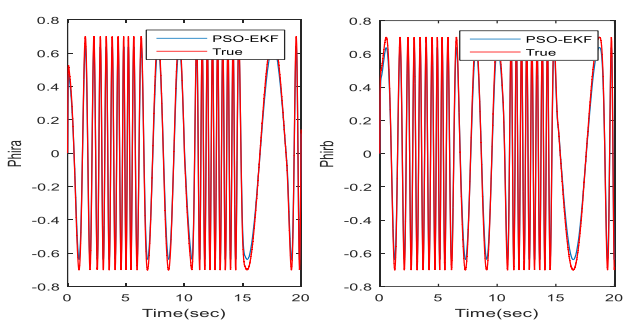

Fig.10. The trajectories of the PSO- EKF and actual rotor fluxes (a) in α axis (b) in β axis

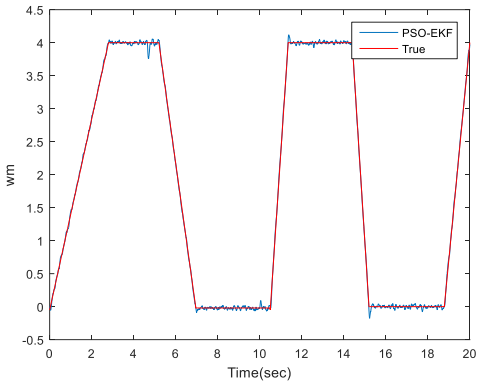

Fig.11. Trajectory of the PSO- EKF and actual motor speed.

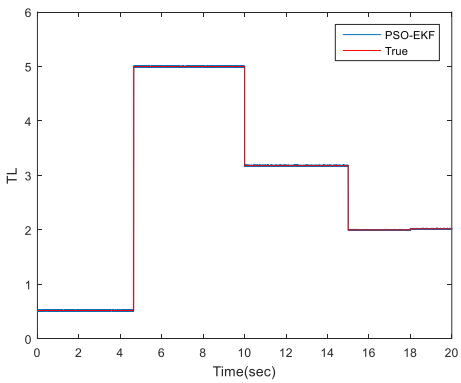

Fig.12. The trajectory of the estimated and actual load torque.

The PSO-EKF adhesion force trajectory is shown in Fig. 13, which is derived from the part of Eq. (4).

The estimated longitudinal creep force makes it possible to determine the level of adhesion that is present between the wheel and the rail. The simulation results show that the proposed approach gives desired output within 5 iterations compared to the trial-and-error approach. In Figs. 9-12, the simulation results relative to the best optimal values of EKF parameters are plotted, which show good convergence between the estimated and actual states. In spite of relatively good convergence between trajectories in the proposed approach, tuning of EKF is time-consuming and challenging.

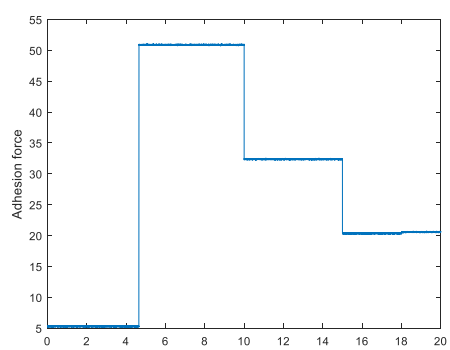

Fig.13. The trajectory of the estimated adhesion force

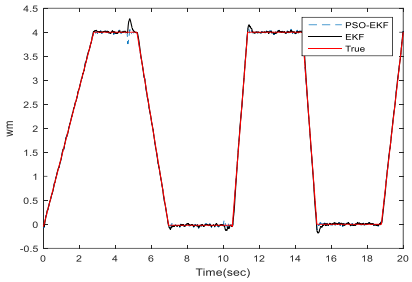

(a)

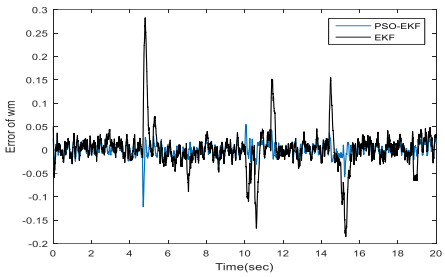

(b)

Fig.14. The speed estimation results for EKF PSO-EKF (a) Estimated speed (b) speed estimation error

A. Performance Comparison

To further show the effectiveness of PSO-EKF, its performance is compared with EKF in Figs.14-15. Considering the resulting estimation performances, the proposed method outperforms EKF because it does not require a priori knowledge of the noises. In addition, in the proposed method, the process covariance is tuned adaptively. The Q matrix in EKF is selected by the trial-and-error method, so it deteriorates the estimation performance of EKF. In addition, it is quite difficult to determine Q that gives sufficient estimation performance by the trial-and-error method.

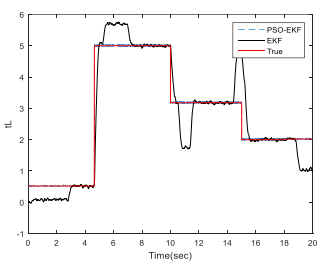

(a)

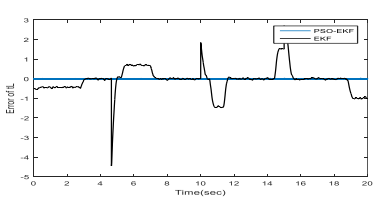

(b)

Fig.15. Load torque estimation results for EKF PSO-EKF (a) Estimated load torque and (b) load torque estimation error

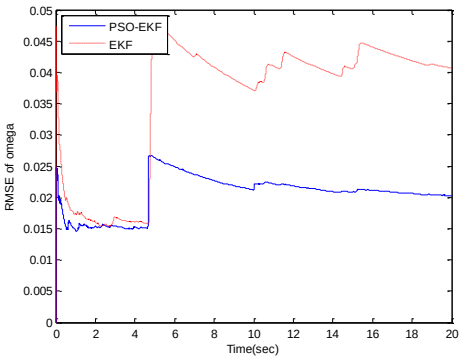

Fig.16. RMSE of Omega over time

To further evaluate the estimations accuracy of the approaches, the root mean square error (RMSE) speed and load torque occurring in estimations are given in Figs. 16-19. RMSE is obtained over 40 Monte Carlo runs. The RMSE of estimations over time is shown in Figs.16 and 17 and their mean and variance are shown in Figs. 18 and 19. Each bar in Figs. 18 and 19 represents the mean and variance of RMSE. It can be found that PSO-EKF outperforms EKF in terms of the mean and variance of RMSE. It can be seen that the RMSE of PSO-EKF is smaller than the RMSE of EKF, so it can be deduced that the speed and load torque estimated by PSO-EKF is closer to their actual values. As a result, the adhesion force estimated using PSO-EKF is more accurate.

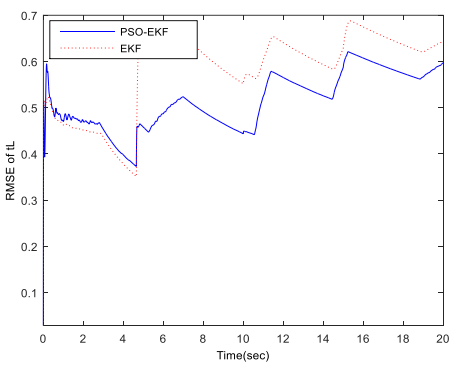

Fig.17. The RMSE of the load torque over time

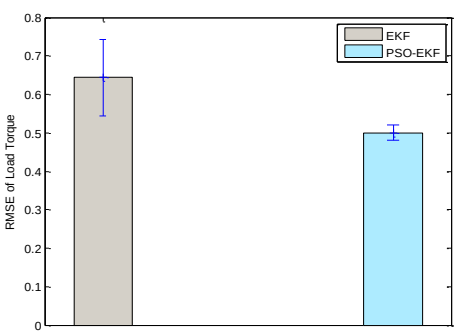

Fig.18. The RMSE of the load torque

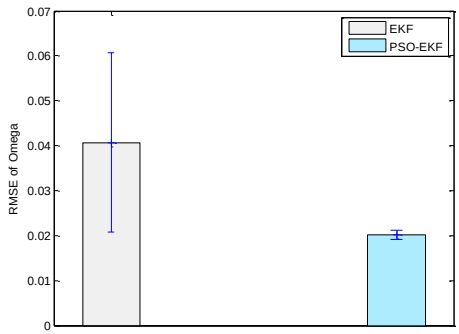

Fig.19. The RMSE of Omega

TABLE3
RUNNING TIME FOR EKF AND PSO-EKF

Method	Running Time(Sec)
EKF	15
PSO-EKF	20

To provide a comprehensive comparison of the methods, we provide the computational time for each method in Table 3. It shows that the cost for this improvement is in the slightly increased computational load in PSO EKF. However, this fact is insignificant if the poor performance of EKF is taken into account.

VI. Conclusions

EKF is based on system linearization and requires a Jacobian matrix in this process. The calculation of the Jacobian matrix is a difficult and error-prone operation. As we saw in the simulation results of this paper, EKF does not have the necessary accuracy in estimating the variables. This is due to the high dependence of the output on the values of noise and process covariance matrices, which can be mentioned as another drawback of this type of filter. A PSO-EKF is proposed to make an effective re-adhesion estimator. The PSO- EKF estimator's performance was evaluated by comparing the actual and estimated values of load torque, motor speed, rotor flux, and stator current. Then, according to the relationship between the torque and longitudinal creep force, the motor torque and adhesion force were calculated. It was observed that PSO-EKF estimated the states with low error values when the wheel-rail contact conditions varied. In this course, different creep curves corresponding to different contact conditions are utilized and the estimation results are found accurate and desirable. Beneficial implications of the proposed estimator include improvement in the performance of the re-adhesion controller, creepage reduction, and maximum traction achievement. Meanwhile, the proposed PSO-EKF estimator has superiority in estimation when the wheel-rail contact conditions change. Despite these advantages, one of the major problems of this type of estimator is that tuning the covariance matrices of process and measurement noise is time-consuming. An appropriate hybrid model such as GA-PSO-EKF may provide more flexible and fast convergence and less computational time than the individual models. This estimator shall be simulated and implemented in future works to improve the estimation accuracy and save time.

REFERENCES

[1] J. Zhou, M. Wu, C. Tian, et al., "Experimental investigation on wheel–rail adhesion characteristics under water and large sliding conditions." Industrial Lubrication and Tribology, Vol. 73, No. 2, pp. 366-372. 2021.

[2] H. Chen, T. Furuya, S. Fukagai, et al., "Wheel slip/Slide and low adhesion caused by fallen leaves." wear, Vol. 446–447, 203187, 2020.

[3] M. Harmon, R. Lewis "Review of top of rail friction modifier tribology. Tribology Materials, Surfaces & Interfaces." pp.150–162, 2016.

[4] Y. Lyu, E. Bergseth, U. Olofsson "Open system tribology and influence of weather condition. Scientific Reports." 6:32455, 2016.

[5] H. Chen, H. Tanimoto, "Experimental observation of temperature and surface roughness effects on wheel/rail adhesion in wet conditions." Int J Rail Transportation. 6:101–112, 2018.

[6] U. Olofsson, Y. Lyu, "Open system tribology in the wheel–rail contact—a literature review." Appl Mechanics Rev. 69:60803, 2017.

[7] M. Shen., Y. Qin, D. Ji, et al. "Role of ambient temperature in the adhesion and damage characteristics of wheel/rail interface during rolling-sliding contact." wear, Vol. 506–507, 204458. 2022.

[8] M. Spiryagin, C. Cole, YQ Sun, et al. "General modelling techniques. Design and simulation of rail vehicles." Boca Raton, Florida: CRC Press/Taylor and Francis. pp. 79–95, 2014.

[9] H. Chen, M. Ishida, A. Namura, et al. "Estimation of wheel/rail adhesion coefficient under wet condition with measured boundary friction coefficient and real contact area", Wear, Vol. 271, pp. 32–39, 2011.

[10] I. Hussain, T. Mei, and Ritchings, "R. Estimation of wheelrail contact conditions and adhesion using the multiple model approach", Vehicle System Dynamics, Vol. 51, pp. 32–53, 2013.

[11] S. Strano, and M. Terzo, "On the real-time estimation of the wheel-rail contact force by means of a new nonlinear estimator design model", Mechanical Systems and Signal Processing, Vol. 105, pp. 391–403, 2018.

[12] H. Schwartz and R. Kresse, "Implementation of an advanced wheel creep control with searching strategy on a light rail vehicle," European Conference on Power Electronics and Applications, Nagaoka, Japan, pp. 3.434–3.438, 1997.

[13] I. Yasuoka, T. Henmi,Y. Nakazawa, and I. Aoyama, "Improvement of re-adhesion for commuter trains with vector controltraction inverter," Proceedings of the Power Conversion Conference, pp. 51–56, 1997.

[14] T. Watanabe and A. Yamanaka, T. Hirose, K. Hosh, and S. Nakamura, "Optimisation of readhesion control of Shinkansen trains with wheel–rail adhesion, prediction, Proceedings of the Power Conversion Conferecne," Nagaoka, Japan, pp. 47–50, 1997.

[15] M. Spiryagin, P. Wolfs, Q. Wu, et al. “Rail Cleaning Process and its Influence on Locomotive Performance.” Joint Rail Conference (JRC2017). Philadelphia, PA: ASME. Apr 4, 2017.

[16] M. Spiryagin, C. Cole, YQ. Sun, “Adhesion estimation and its implementation for traction control of locomotives.” Int J Rail Transportation, pp.187–204, 2014.

[17] P. Pichlík, J. Zděnek, “Adhesion force detection method based on the kalman filter for slip control purpose,” Automatika – Journal for Control, Measurement, Electronics, Computing and Communications, Vol. 57, No. 2, pp. 405-415, 2016.

[18] Y. Zhao, B. Liang, “Re-adhesion control for a railway single wheelset test rig based on the behaviour of the traction motor,” Vehicle Syst Dyn, Vol. 51, No. 1, pp. 173–1185, 2013.

[19] A. Kawamura, , K. Takeuchi, T. Furuya, et al., “Measurement of Tractive Force and the New Maximum Tractive Force Control by the Newly Developed Tractive Force Measurement Equipment,” IEEJ Transactions on Industry Applications, Vol. 123, No. 8, pp. 885-893, 2003.

[20] Y. Matsumoto, N. Eguchi, A. Kawamura, “Novel Re-Adhesion Control for Train Traction System of The Shinkansen with The Estimation of Wheel-to-Rail Adhesive Force,” IECON'01, 27th Annual Conference of the IEEE Industrial Electronics Society (Cat. No.37243), 29 Nov.-2 Dec. Denver, CO, USA, Vol. 2, pp. 1207-1212, 2001.

[21] Y. Zhao, B. Liang, “Re-adhesion control for a railway single wheelset test rig based on the behaviour of the traction motor”, Vehicle System Dynamics, Vol 51, No. 8, pp. 1173-1185, 2013.

[22] S. Wang, J. Xiao, J. Huang, Sheng, H., “Locomotive Wheel Slip Detection Based on Multi-Rate State İdentification of Motor Load Torque”, Journal of the Franklin Institute, Vol. 353, No. 2, pp. 521-540, 2016.

[23] M. Barut, O. Bogosyan, M. Gokasan, “EKF Based Estimation for Direct Vector Control of Induction Motors”, IEEE 28th Annual Conference of the Industrial Electronics Society, Sevilla, Spain, pp.1710-1715. November 2002.

[24] L. Zhang, Y. Zhang, Z. Liu, et al, “Application of Genetic Algorithms in EKF for Speed Estimation of an Inducion Motor”, Proc. on IEEE Power Electronics Specialist Conference, Acapulco, Mexico, Vol. 1, pp. 345-349, 15-19, June 2003.

[25] C. Schwarz, A. Keck, “Observer Synthesis for the Adhesion Estimation of a Railway Running Gear”. ELSEVIER, Vol 52, Issue 15, pp. 319-324, 2019.

[26] M. Barut, S. Bogosyan, and M. Gokasan, “Speed-Sensorless Estimation for Induction Motors Using Extended Kalman Filters,” IEEE Transactions on Industrial Electronics, Vol. 54, No. 1, pp. 272–280, Feb. 2007.

[27] M. Barut, R. Demir, E. Zerdali, and R. Inan, “Real-Time Implementation of Bi Input-Extended Kalman Filter-Based Estimator for Speed-Sensorless Control of Induction Motors,” IEEE Transactions on Industrial Electronics, Vol. 59, No. 11, pp. 4197–4206, Nov. 2012.

[28] R. Inan and M. Barut, “Bi input-extended Kalman filter-based speed-sensorless control of an induction machine capable of working in the field-weakening region,” Turk J Elec Eng & Comp Sci, Vol. 22, No. 3,pp. 588–604, Apr. 2014.

[29] E. Zerdali and M. Barut, “Novel version of bi input-extended Kalman filter for speed-sensorless control of induction motors with estimations of rotor and stator resistances, load torque, and inertia,” Turk. J. Electr.Eng. Comput. Sci., Vol. 24, No. 5, pp. 4525–4544, 2016.

[30] S. H. Moosapour, M. Asadollahi, and S. S. Moosapour, “State Estimation in a Power System by Utilizing EKF and UKF.” 28th International Power System Conference, Tehran, 2014.

[31] K. L. Shi, T. Chan, Y. Wong, and S. Ho, “Speed estimation of an induction motor drive using an optimized extended Kalman filter,” IEEE Transactions on Industrial Electronics, Vol. 49, No. 1, pp. 124–133, Feb.2002.

[32] N. Salvatore, A. Caponio, F. Neri, S. Stasi, et al, “Optimization of Delayed-State Kalman-Filter-Based Algorithm via Differential Evolution for Sensorless Control of Induction Motors,” IEEE Transactions on Industrial Electronics, Vol. 57, No. 1, pp. 385–394, Jan. 2010.

[33] E. Zerdali and M. Barut, “The Comparisons of Optimized Extended Kalman Filters for Speed-Sensorless Control of Induction Motors,” IEEE Transactions on Industrial Electronics, Vol. 64, No. 6, pp. 4340–4351, Jun. 2017.

[34] A. Almagbile, J. Wang, and W. Ding, “Evaluating the Performances of Adaptive Kalman Filter Methods in GPS/INS Integration,” Journal of Global Positioning Systems, Vol. 9, No. 1, pp. 33–40, Jun. 2010. Using an Interfacing Multiple-Model Extended Kalman Filter,” IEEE Transactions on Power Electronics, Vol. 29, No. 6, pp. 3011–3019, Jun. 2014.

[35] K. Drozdz, “Estimation of the mechanical state variables of the two-mass system using fuzzy adaptive Kalman filter - Experimental study,” in 2015 IEEE 2nd International Conference on Cybernetics (CYBCONF), pp. 455–459, Jun. 2015.

[36] Z. Yin, G. Li, Y. Zhang, et al, “A Speed and Flux Observer of Induction Motor Based on Extended Kalman Filterand Markov Chain,” IEEE Transactions on Power Electronics, Vol. 32, No. 9, pp. 7096–7117, Sep. 2017.

[37] Z. Yin, L. Xiao, X. Sun, et al, “A speed and flux estimation method of induction motor using fuzzy extended kalman filter,” in Electronics and Application Conference and Exposition (PEAC), 2014 International, pp. 693–698, Nov. 2014.

[38] C. P. Ward, R. M. Goodall, R. Dixon, et al. “Adhesion estimation at the wheel–rail interface using advanced model-based filtering. Vehicle System Dynamics,” Vol. 50, pp.1797–1816, 2012.

[39] P. Hubbard, C. Ward, R. Goodall, et al. ‘Real time detection of low adhesion in the wheel/rail contact. Proceedings of the Institution of Mechanical Engineers,” Part F: Journal of Rail and Rapid Transit, Vol. 227, pp. 623–634, 2013

[40] S. Iwnicki, editor. Handbook of railway vehicle dynamics. Boca Raton, FL: CRC Press; 2006.

[41] M. Spiryagin, C. Cole, YQ. Sun, et al. “Design and simulation of rail vehicles, ground vehicle engineering series,” Boca Raton, FL: CRC Press; 2014.

[42] C. Weidemann, “State-of-the-art railway vehicle design with multibody simulation,” J Mech Systems Transport Logist, pp. 12–26; 2010.

[43] A. Steimel, “Electric traction–motive power and energy supply: basics and practical experience,” Munich: Oldenbourg Industrieverlag; 2008.

[44] R. Mathew, F. Flinders, and W. Oghanna, "Locomotive 'total systems' simulation using SIMULINK," Proceedings of international conference on electric railways in a United Europe; Amsterdam, pp. 202–206, 1995.
[45] O. Polach, "Creep forces in simulations of traction vehicles running on adhesion limit," Wear. 258:992–1000; 2005.
[46] EAH. Vollebregt, "Numerical modeling of measured railway creep versus creep-force curves with CONTACT," Wear. Vol. 314, pp. 87–95; 2014.
[47] M. Spiryagin, KS. Lee, HH. Yoo, et al, "Modeling of adhesion for railway vehicles." J Adhes Sci Technol. pp.1017–1034; 2008.
[48] M. Spiryagin, O. Polach, and C. Cole, "Creep force modelling for rail traction vehicles based on the Fastsim algorithm," Veh Syst Dyn.;51(11):1765–1783, 2013.
[49] JJ. Kalker, "A fast algorithm for the simplified theory of rolling contact," Veh Syst Dyn.Vol.1, pp.1–13; 1982.
[50] O. Polach, "Influence of locomotive tractive effort on the forces between wheel and rail," Veh Syst Dyn. pp.7–22; 2001.
[51] M. Spiryagin, S. Simson, C. Cole, et al. "Co-simulation of a mechatronic system using Gensys and Simulink," Veh Syst Dyn, Vol. 50, pp. 495–507, 2012.
[52] HP. Kotz, "A toolkit for simulating mechatronics in railway vehicles," Simpack User Meeting 2003, Germany, 2003. Available from: http://www.simpack.com/fileadmin / simpack/doc/usermeeting03/um03-siemens_kotz.pdf.
[53] M. Spiryagin, A. George, YQ. Sun, et al, "Investigation on the locomotive multibody modelling issues and results assessment based on the locomotive model acceptance procedure," J Rail Rapid Transit; Vol. 227, Issue 5, pp. 453–468, 2013.
[54] O. Polach, A. Böttcher, D. Vannucci, et al, "Validation of simulation models in the context of railway vehicle acceptance," J Rail Rapid Transit. October 28, 2014; published online before print.
[55] Y. Zhang, S. Wang, G. Ji, "A comprehensive survey on particle swarm optimization algorithm and its applications," Math. Probl. Eng. 2015.
[56] R. Eberhart, J. Kennedy, "A new optimizer using particle swarm theory," Micro Machine and Human Science, MHS 95., Proceedings of the Sixth International Symposium on, 1995, pp. 39–43, 1995.
[57] M. M. Rizi, S. Abazari, N, Mahdian, "Dynamic Stability Improvement of Power System with Simultaneous and Coordinated Control of DFIG and UPFC using LMI," Vol. 4, Issue 3, pp. 341-353, 2021. Available from: https://doi.org/10.22111/ieco.2021.37604.1340
[58] Q. Wu, C. Cole, T. McSweeney, "Applications of particle swarm optimization in the railway domain," Int. J. Rail Transp. Vol. 4, Issue 3, pp.167–190, 2016.
[59] A. Onat, P. Voltr, "Particle swarm optimization based parametrization of adhesion and creep force models for simulation and modelling of railway vehicle systems with traction," ELSEVIER, Vol. 99, 102026, 2020.
[60] A. Zirek, A. Onat, "A novel anti-slip control approach for railway vehicles with traction based on adhesion estimation with swarm intelligence," Springer, Vol. 28, Issue 4, pp. 346–364, 2020.
[61] M. Barut, S. Bogosyan, and M. Gokasan, "EKF Based Sensorless Direct Torque Control of IMs in The Low Speed Range", Proceedings of the IEEE International Symposium on Industrial Electronics, 2005, ISIE 2005, Dubrovnik, Croatia, pp. 20-23 June 2005.
[62] O. Polach, "A Fast Wheel-Rail Forces Calculation Computer," Veh. Syst. Dyn. Suppl, Vol. 33, pp. 728–739, 1999.
[63] J. Kalker, "On The Rolling Contact of Two Elastic Bodies in The Presence of Dry Friction," Wear, Vol. 11, Issue 4, pp. 303, 1968.
[64] KL. Shi, YK. Wong, and SL. Ho, "Speed estimation of an induction motor drive using an optimized extended Kalman filter.," IEEE Trans. On Industrial Electronics, Vol. 49, pp. 124-133, 2002.

APPENDIX A: The pseudo code for PSO-EKF

1. Initialize particles and the parameters of PSO Do

2. Reconstruct the matrices Q, R

3. Run EKF

3.1 Find Jacobian matrices $\mathbf{F_e(k)}$

$$F_e(k) = \frac{\partial f_e(x_e(k).u_e(k))}{\partial x_e(k)}\Big| (\hat{x}_e(k).\hat{u}_e(k))$$

3.2 Prediction of error covariance matrix

$$P^-(k+1) = F_e(k)P_k(k)(F_e(k))^T + F_u(k) D_u(k)(F_u(k))^T + Q(k)$$

3.3 Calculation of Kalman gain matrix

$$K(k) = P^-(k+1)H^T(HP^-(k+1)H^T + R(k))^{-1}$$

3.4 Update state and error covariance

$$\hat{x}_e(k+1) = \hat{f}_e\big(x_e(k).\hat{u}_e(k)\big) + K(k)(z(k) - H\hat{x}_e(k))$$

$$P(k+1) = (I - K(k)H)P^-(k+1)$$

4. Optimization Q and R by PSO

4.1 Evaluate fitness of particles

$$J = \frac{1}{N}\sum_{k=0}^{N}\|i_s(k) - \hat{i}_s(k)\|_2^2$$

4.2 Update particle velocity and position

$$v_i(k+1) = w.v_i(k) + c_1.r_1(k).(p_i(k) - x_i(k)) + c_2.r_2(k).(p_g(k) - x_i(k))$$

$$x_i(k+1) = x_i(k) + v_i(k+1)$$

Until Maximum iteration

Ramazan Havangi received his M.S. and Ph.D. degrees from the K.N. Toosi University of Technology, Tehran, Iran in 2003 and 2012, respectively. He is currently an Associate Professor of control systems with the Department of Electrical and Computer Engineering at the University of Birjand, Birjand, Iran. His main research interests are inertial navigation, integrated navigation, estimation and filtering, evolutionary filtering, simultaneous localization and mapping, fuzzy, neural network, and soft computing.

Maryam Moradi was born in Tehran, Iran. She received her B.S. degree in Control Engineering from Gonabad Azad University, Gonabad, Iran in 2008, and her M.S. degree in Telecommunications Engineering from the Faculty of Engineering at the University of Sistan

and Baluchestan, Zahedan, Iran in 2015. Since 2018, she has been a Ph.D. student in Control Engineering at the Faculty of Engineering, the University of Birjand, Birjand, Iran. In 2019, she joined the University of Applied Sciences & Technology as a teacher.